CERN-ACC-NOTE-2018-0066
CERN-PBC-Notes-2018-002
KLEVER-PUB-18-01

2018-10-03

mvandijk@cern.ch

Target studies for the proposed KLEVER experiment

M.W.U. van Dijk, M. Rosenthal

Keywords: KLEVER, Physics Beyond Colliders, neutral kaons, FLUKA, Geant, target

Summary

The KLEVER experiment is being proposed to measure the branching ratio $K_L \rightarrow \pi^0 \nu\bar{\nu}$ at the K12 beamline at the CERN SPS. This study presents considerations for the target required for such an experiment, specifically the production angle, target length and material. Geant and FLUKA simulations of a 400 mm beryllium target are benchmarked relative to experimental data, and signal and background production are assessed. Additionally, a simple parametrization representative for a KLEVER type target is presented and tested against these simulations. The parametrization is found to be a reasonable representation for the target under consideration. It is found that the intended change of production angle (2.4 to 8 mrad) has the desired effect of reducing the background, while having only a small effect on the signal. Finally, two additional, higher-Z materials (copper and lead) are explored. It is found that particle production is close to identical to that for beryllium, except for gamma production, where a strong reduction is seen as the material Z is increased.

1 Introduction

Neutral kaon experiments have a long history at CERN. In 1988, the NA31 experiment found the first evidence of direct CP violation in the kaon system. This finding, however, was disputed by the Fermilab experiment E731, which found no such evidence. The issue was settled in 1999, when both successors (NA48 at CERN and KTeV at Fermilab) announced that they had found significant evidence. The NA48 experiment was continued in two further stages, studying in great detail the properties of strange particles. The NA62 experiment started taking data in 2015, to study in detail the extremely rare decay $K^+ \rightarrow \pi^+ \nu\bar{\nu}$, aiming to collect as many as a hundred of these decays. The rarity of this decay sets the scale of difficulty of the project: for every detected decay, another 10^{11} decays need to be rejected, using a combination of hardware, triggering and data analysis techniques.

KLEVER is a planned neutral kaon experiment, to measure the branching ratio of $K_L \rightarrow \pi^0 \nu\bar{\nu}$ at the K12 beamline at the SPS (see (1)). This note will discuss the various aspects of selecting a target suitable for such an experiment, taking under consideration the following variations: target length, proton incident angle and target material. The goal is to give a complete description of the particle production, specifically in terms of neutral kaons (signal) and Λ^0 baryons (expected to be the most important source of potential background). This study is performed with simulated data from FLUKA (see (2), (3)) and G4Beamline (see (4)), a

framework using Geant4 (see (5)), and will only consider the particles as they emerge from the target.

The SPS currently feeds the K12 beamline (leading to the NA62 experiment) with 400 GeV/c protons, and a change in momentum is not currently anticipated. Measuring the particle content emerging from the target takes considerable difficulty, and a very different design for charged and neutral particles. Efforts were undertaken at CERN for measuring the charged particle content of the secondary beam (see (6)) driven by 400 GeV/c protons, and at Fermilab a neutral beamline was constructed in order to measure several of the neutral components (see (7), (8), (9)). The simulated data created with FLUKA and Geant will be benchmarked relative to these sources, before going on to fully quantify the particle production. Data analysis is performed with ROOT (see (10)). For the FLUKA simulation, version FLUKA2017 version 1.0, March 2017 (A. Ferrari) was used. The Geant simulation was created with G4Beamline 3.04, using Geant 4.10.03 and physics list FTFP_BERT.

The goal of this study is three-fold. The first is to benchmark the production of secondary particles using a 400 GeV/c proton beam relative to available data. The second goal is to explore the parameter space available for designing a beamline in terms of the target material, length, and the secondary production angle. The third and final goal is to make available in an easy format the outcomes of these studies, both as a series of histograms and making available the full underlying datasets.

2 The target simulation

2.1 General description

The baseline for the simulation is a simple cylinder, with 400 GeV/c primary protons impinging in the centre of the cylinder. At the far end of the target, a virtual plane is placed, and all particles that cross it are scored. The resulting dataset is split up by particle species. The angle of the secondary particles relative to the primary protons is the parameter of interest. In effect, this means scoring all particles in a ring around the central axis, as displayed in Figure 1.

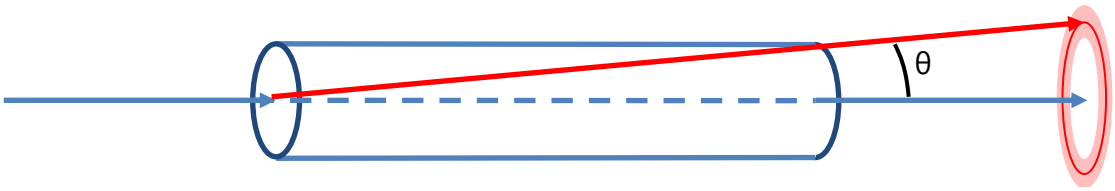

Figure 1: Schematic drawing of particles impinging on a target, showing the solid area for secondary particles emerging at an angle θ

In a realistic scenario, the beam of particles would be tilted relative to the target. It is asserted that, by symmetry, the simulation used is substantially identical, when quantifying a small solid angle, as long as care is taken that emerging secondary particles have travelled the full length of material. This sets the radius of the cylinder to be used. For a particle created at the start of a 400 mm target (the longest taken under consideration), at an angle of 50 mrad, the required radius is slightly over 20 mm. A cylinder radius of 22 mm is used for all simulated targets. The production is then derived per particle species and normalized per incident proton and per solid angle, for a given angle relative to the primary beam. To reduce the computation time, a cut is implemented to remove all particles below 1 GeV/c momentum.

The particles under study in KLEVER will be neutral kaons. These particles can be described in terms of the particle / antiparticle paradigm, or alternatively in terms of their CP eigenstates (K_S and K_L or K short and K long). In Geant, it is possible to directly query whether a particle manifests as short or long. In FLUKA, particles are propagated in the mass eigenstate, with varying components describing the K_S and K_L content of that particle. These components are normalized:

$$A_S^2 + A_L^2 = 1$$

For counting the K_S component of the beam in FLUKA, a sum is made over the squared amplitudes A_S for both K^0 and $\overline{K^0}$ (identical for K_L). This is then propagated identical to all other particles.

2.2 Data for benchmarking

A literature review was undertaken to find sources containing data relevant to the study at hand, and four sources were selected. The first of these is a CERN yellow report (see (6)), which has long served as the standard for estimating particle production from the beryllium North Area targets. The data will be compared to the simulation in Section 4. In addition to the data, a parametrization is stated in this paper (from here on referred to as the Atherton parametrization). This parametrization is used to describe production of charged secondaries for reasonably high momenta (> 60 GeV/c) for a thin target. The data measured by Atherton et al. was also used to construct a second parametrization (see (11)) adjusted for thick targets, which is much closer to the situation relevant to KLEVER. The simulated data will also be compared to these two parametrizations.

The second (see (7)) and third (see (8)) sources were chosen because they contain measurements of the strange content of the beam, measured for beryllium, copper and lead targets. These measurements were undertaken at the M2 beamline at Fermilab. They describe measurements of the interaction cross section for K_S, Λ^0, $\overline{\Lambda^0}$, Ξ^0 and $\overline{\Xi^0}$, for selected production angles. These measurements resulted in an interaction cross section, which can be compared to the simulated data, for a short target. An overview of strange particle production is found in (12), a more complete review of particle production measurements can be found in (13).

The fourth and final source used for this study (9) describes a series of measurements of the inclusive cross section for neutrons on several target materials, using 400 GeV/c protons, also performed at the M2 beamline at Fermilab.

The sources mentioned above, excepting (6), all measured the invariant cross section as a function of production angle and secondary momentum. The invariant cross section $E\frac{d^3\sigma}{dp^3}$ relates to the double differential cross section as follows:

$$E\frac{d^3\sigma}{dp^3} = \frac{p^2}{E}\frac{d^2N}{dpd\Omega}$$

In the following sections the double differential cross section is used, describing the number of particles produced per proton on target, at a certain momentum and production angle.

3 Benchmarking the target simulation

Results from the simulation are purposely split into two parts. The first will compare the production of particles in Geant and Fluka relative to that expected from applying the interaction cross sections to a relatively thin target (40 mm beryllium or equivalent, about 10% of a nuclear interaction length). Using a thin target implies that momentum loss of particles within the target can be assumed to be small. Additionally, it means that the production of tertiary particles from secondaries can be assumed to be negligible. With the conclusions drawn from the production process in place, the full-length target (expected to be 400 mm beryllium or equivalent) is used for assessing the full particle production.

3.1 Results using a thin target

3.1.1 Charged particles

The data collected in Atherton et al. spans the momentum regime of 60 to 300 GeV/c secondary momentum, for positive and negative pions, kaons and protons. The data has been recorded at two values of transverse momentum, 0 and 0.5 GeV/c. The data from the simulations was processed to show the same parameter space, cutting and normalizing to +/- 0.1 GeV/c transverse momentum around the selected values. The Atherton parametrization (6) is stated as:

$$\frac{d^2N}{dpd\Omega} = A\left[\frac{(B+1)}{p_0}\left(\frac{p}{p_0}\right)^B\right]\left[\frac{2Cp^2}{2\pi}e^{-C(p\theta)^2}\right] \qquad \text{(for protons)}$$

$$\frac{d^2N}{dpd\Omega} = A\left[\frac{B}{p_0}e^{-B\frac{p}{p_0}}\right]\left[\frac{2Cp^2}{2\pi}e^{-C(p\theta)^2}\right] \qquad \text{(for other charged hadrons)}$$

The values of the parameters A, B and C of the Atherton parametrization are shown in Table 1.

	A	B	C
p	0.8	-0.6	3.5
$\bar{p}$	0.06	16.0	3.0
π^+	1.2	9.5	5.0
π^-	0.8	11.5	5.0
K^+	0.16	8.5	3.0
K^-	0.10	13.0	3.5

Table 1: Atherton parameters

The Atherton parametrization describes the number of particles generated per interacting proton, per solid angle (sterad), per GeV/c. The fraction of interacting protons (including secondary reabsorption) relative to the total number of protons on target is a scaling factor. For a target of length L and made of a material with nuclear interaction length λ_I it can be described as:

$$\frac{N_{int}}{N_{tot}} = \frac{L}{\lambda_I} e^{-\frac{L}{\lambda_I}}$$

Figure 2 shows the Atherton parametrization (continuous line), Atherton data (symbols), FLUKA simulated data (broken histogram) and Geant simulated data (continuous histogram) on a logarithmic scale. For the simulations, 100M primary protons at 400 GeV/c were used on a 40 mm thick beryllium target. The agreement between the data and the simulation is in most cases reasonable. In some cases there is a better agreement with Geant (e.g. π^-), in some cases there is better agreement with FLUKA (e.g. K^+).

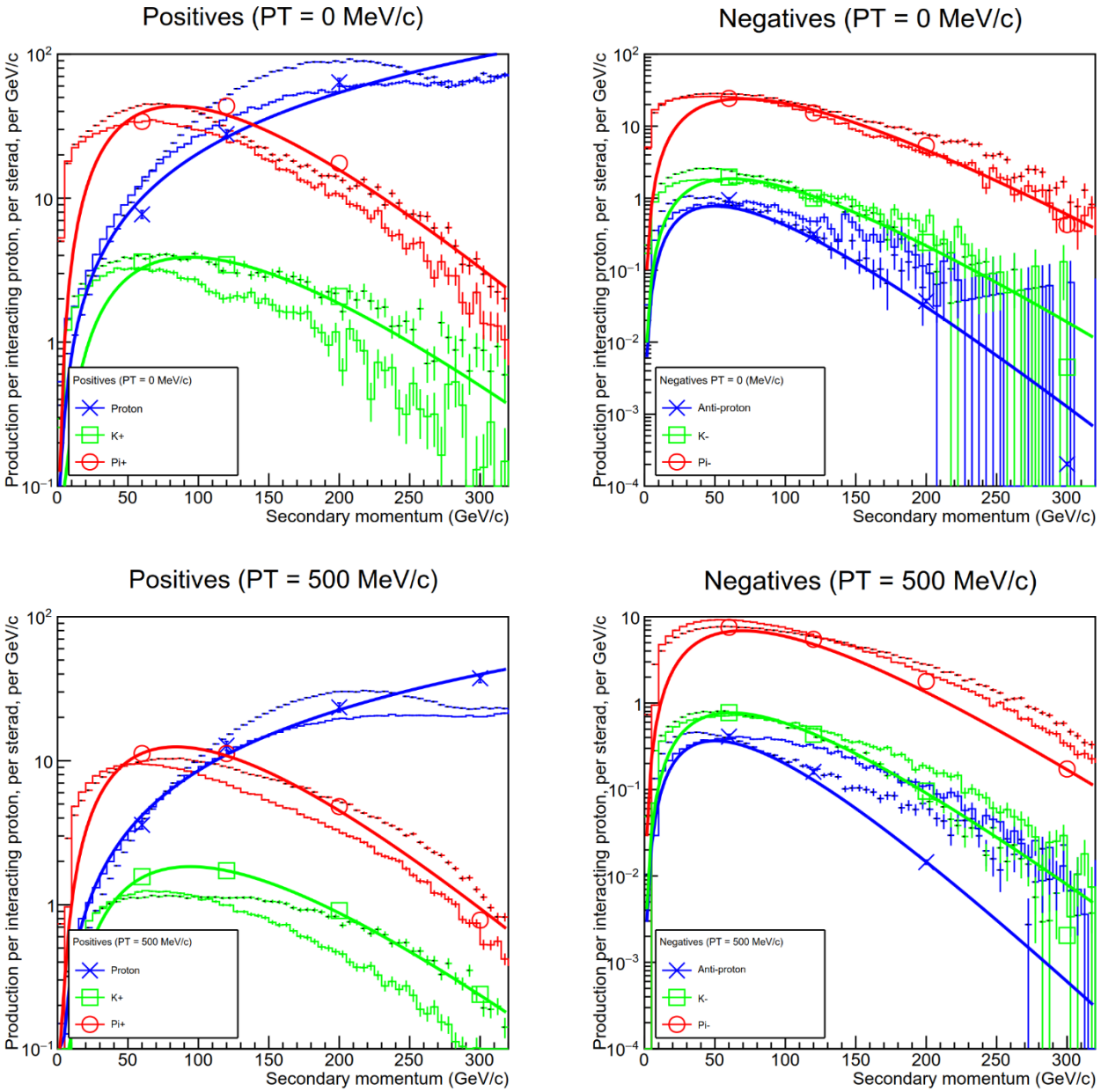

Figure 2: Measured data (symbols), Geant simulated data (continuous histogram), FLUKA simulated data (broken histogram) and the Atherton parametrization for charged particles, at 0 and 0.5 GeV/c pT (6)

The Atherton parametrization was constructed as a pragmatic, continuous representation with good agreement to data. Because of the sparsity of the data, no strong conclusions can be drawn on its quality - however it does not replicate the simulation well, especially at low momenta. Due to the form of the parametrization, refitting the simulated parameters with floating

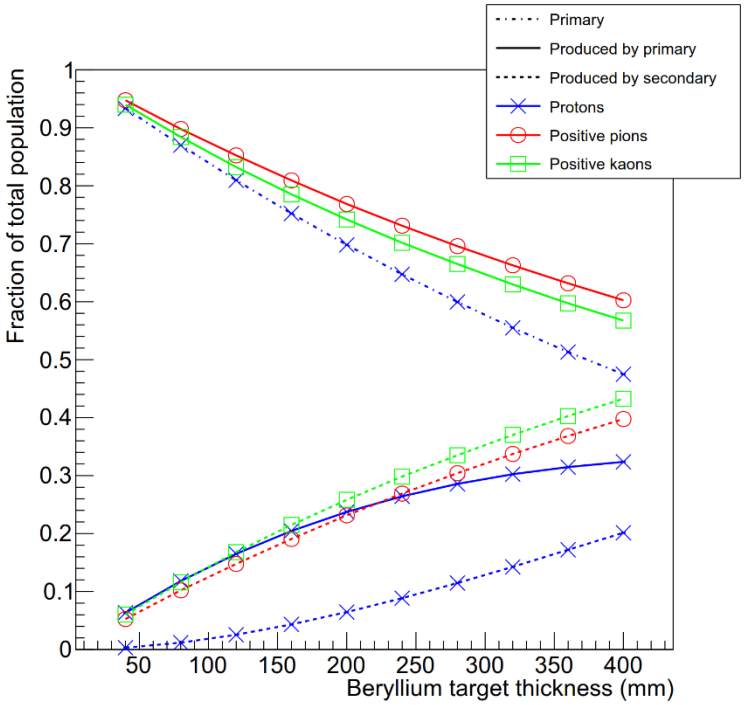

Figure 3: Origin of positive charged particles, as a function of target thickness (FLUKA)

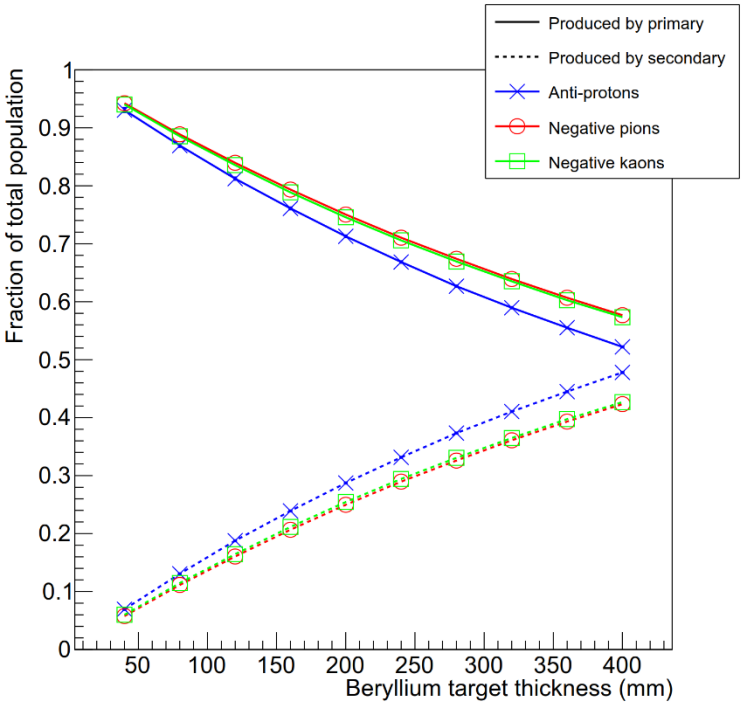

Figure 4: Origin of negative charged particles, as a function of target thickness (FLUKA)

parameters does not improve the fit to a point where it can be said to be representative of the simulated data. This becomes yet more apparent for a thick target, where non-primary particles give additional production, and where momentum losses need to be taken into account. In Figure 3 and Figure 4, the fractions of particles generated by primaries and secondaries are shown as a function of the target thickness, counting all particles with an angle less than 10 mrad relative to the primary axis. For a thin 40 mm beryllium target, for the charged particles described above, about 5% is generated from a secondary (or later generation) particle. For a 400 mm target, this is around 40%.

For a thick target, the Atherton parametrization does not represent the particle populations well, in large part due to the high fraction of particles being produced by secondaries. A new parametrization to fill this role instead will be discussed in Section 3.2.

3.1.2 Neutral particles

In addition to charged particle data comparison done in the previous section, it is imperative to also benchmark the production of neutral particles. A series of experiments has been performed at Fermilab measuring the production cross sections for K_S and Λ^0 baryons (7), (8) and neutrons (9). The comparisons with the simulations are shown in Figure 5, Figure 6, Figure 7 and Figure 8. As for the charged particles before, the comparison is made using 100M primary protons at 400 GeV/c momentum impinging on a 40 mm beryllium target. In the simulations, for each production angle the particles within +/- 0.5 mrad of that angle are counted. The resulting numbers are normalized relative to the solid area of that angular space. The invariant cross sections listed in the data are transformed into absolute productions per proton on target, per solid area (in microsteradian).

For fundamental reasons the production of K_S and K_L are equal, and thus benchmarking the production of K_S should also give a reasonable impression of the quality of the K_L generation.

The agreement between the data and both simulations is mostly good. The shape in the spectrum shows some differences between Geant and FLUKA, but significant is not expected. Significant disagreement between the simulation and the data is found only at a very high production angle (20 mrad).

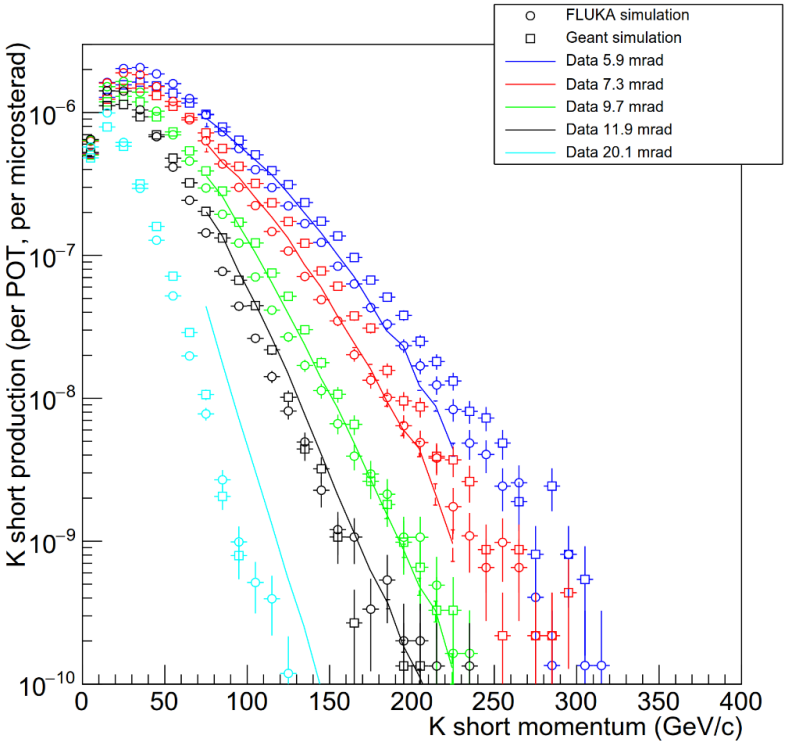

Figure 5: Production of K_S as measured (solid lines, data from (7)) and as simulated in FLUKA and Geant

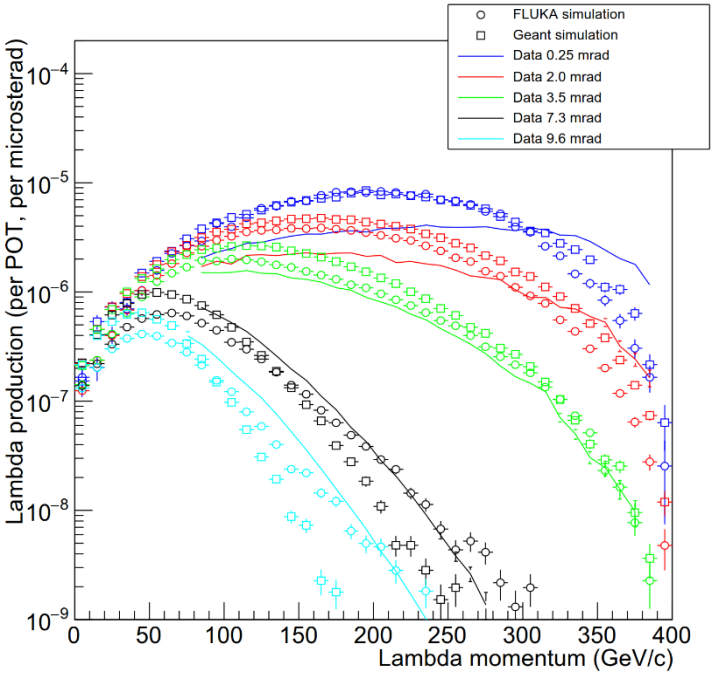

Figure 6: Production of Λ^0 as measured (solid lines, data from (8)) and as simulated in FLUKA and Geant

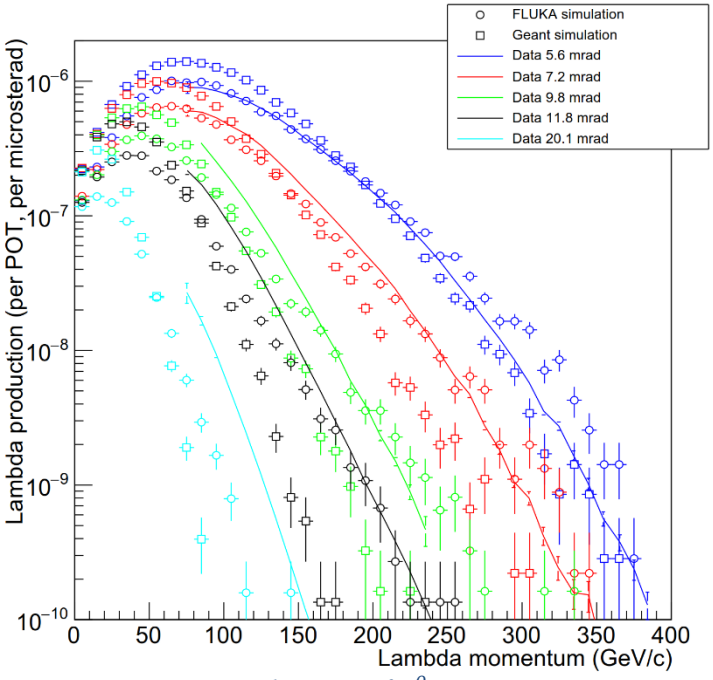

Figure 7: Production of Λ^0 as measured (solid lines, data from (7)) and as simulated in FLUKA and Geant

The production of Λ^0 baryons (Figure 6 and Figure 7) shows disagreements between the data and the simulation, mostly at lower angles. The momentum spectra observed in data at low angles is significantly harder than it is in simulation. At intermediate production angles (about 3.5 to 12 mrad), the Λ^0 momentum spectrum more closely resembles that of the simulation. At large angles, there is again a large discrepancy.

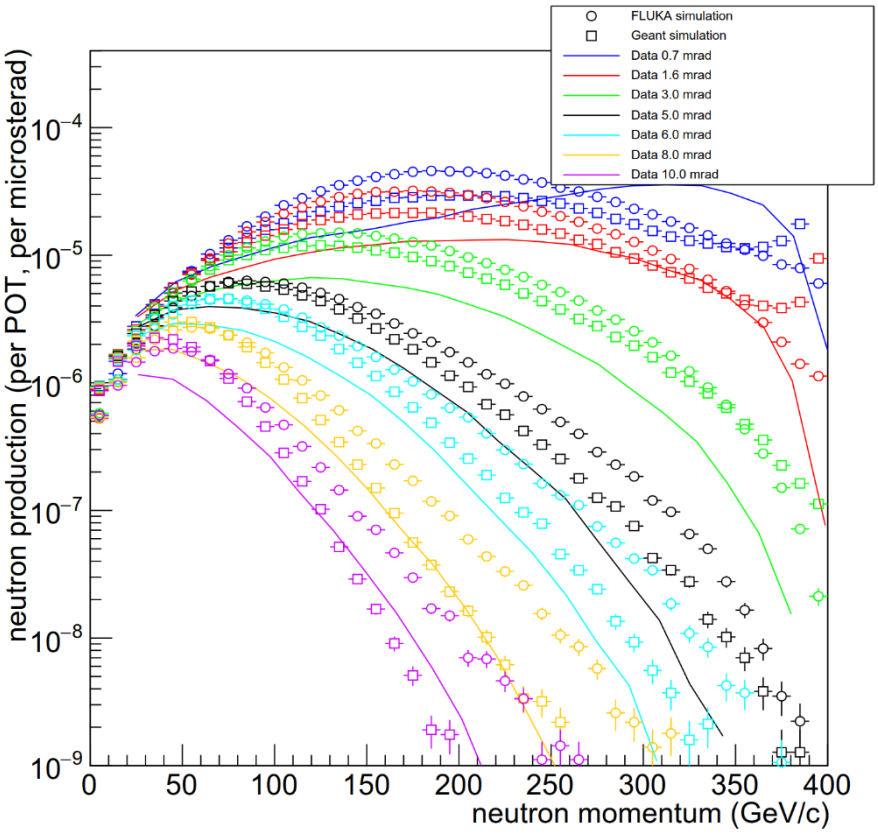

Figure 8: Production of neutrons as measured (solid lines, data from (9)) and as simulated in FLUKA and Geant

Several features stand out in the comparison of the neutron spectra. A large difference is observed between FLUKA and Geant at low angles and high momenta, most likely caused by a difference in the likelihood of charge exchange occurring (conversion of proton to neutron in target with minimal momentum loss). It is unclear what the basis for this difference is. While this is a clear disagreement between FLUKA and Geant, the expectation is that KLEVER will be operated at production angles where this difference is not critical.

As with production of the Λ^0 baryon, the spectrum observed in data at low angles is significantly harder than it emerges from the simulation. Finally, it appears that the total neutron production in simulation is overestimated relative to the data. It is unclear what the source of these discrepancies could be.

The last source of background taken under consideration is Λ^0 regeneration from hyperons. Given that there are several species (notably Ξ particles) that have a large branching fraction to Λ^0, these could regenerate the Λ^0 population downstream of the target. The sum total of Ξ particles at 8 mrad is about 7% of the Λ^0 population, but with significantly lower momenta on average and tailing off at high momentum much more quickly. It is expected that addressing the background from Λ^0 baryons will also sufficiently address that sourced from other hyperons.

3.2 A new parametrization of particle momentum distributions for a thick target

For generating particle momentum distributions with minimal difficulty, the convenience of a parametrization cannot be overstated. To this end, the following parametrization has been used (11), which will henceforth be referred to as the Malensek parametrization:

$$\frac{d^2N}{dpd\Omega} = BX\frac{(1-X)^A(1+5e^{-DX})}{\left(1+{(p\theta)^2}/{C}\right)^4} \quad \text{with} \quad X = \frac{p}{E_0}$$

In the original paper, the parametrization was computed for and compared to the data from the Atherton paper for a thick (400 mm) beryllium target. As is clear from the functional form, it provides a description of the full angular and momentum phase space simultaneously. The same simulated datasets were used (based on FLUKA and Geant), and a fit was made (using the ROOT analysis framework (10)) to the full two-dimensional histogram using the Malensek parametrization. The fit was made for all particle species, including neutrals. The fitted phase space is 0 to 300 GeV/c momentum for protons and neutrons, and 0 to 400 GeV/c momentum for all other particles. The angular phase space used for the fit is 0 to 20.5 mrad. The initial values for the parameters were seeded with the values in the paper where available. Figure 9 and Figure 10 show the fit results for a selection of production angles and particles. A full table of the fitted parameters is made available in Appendix A.

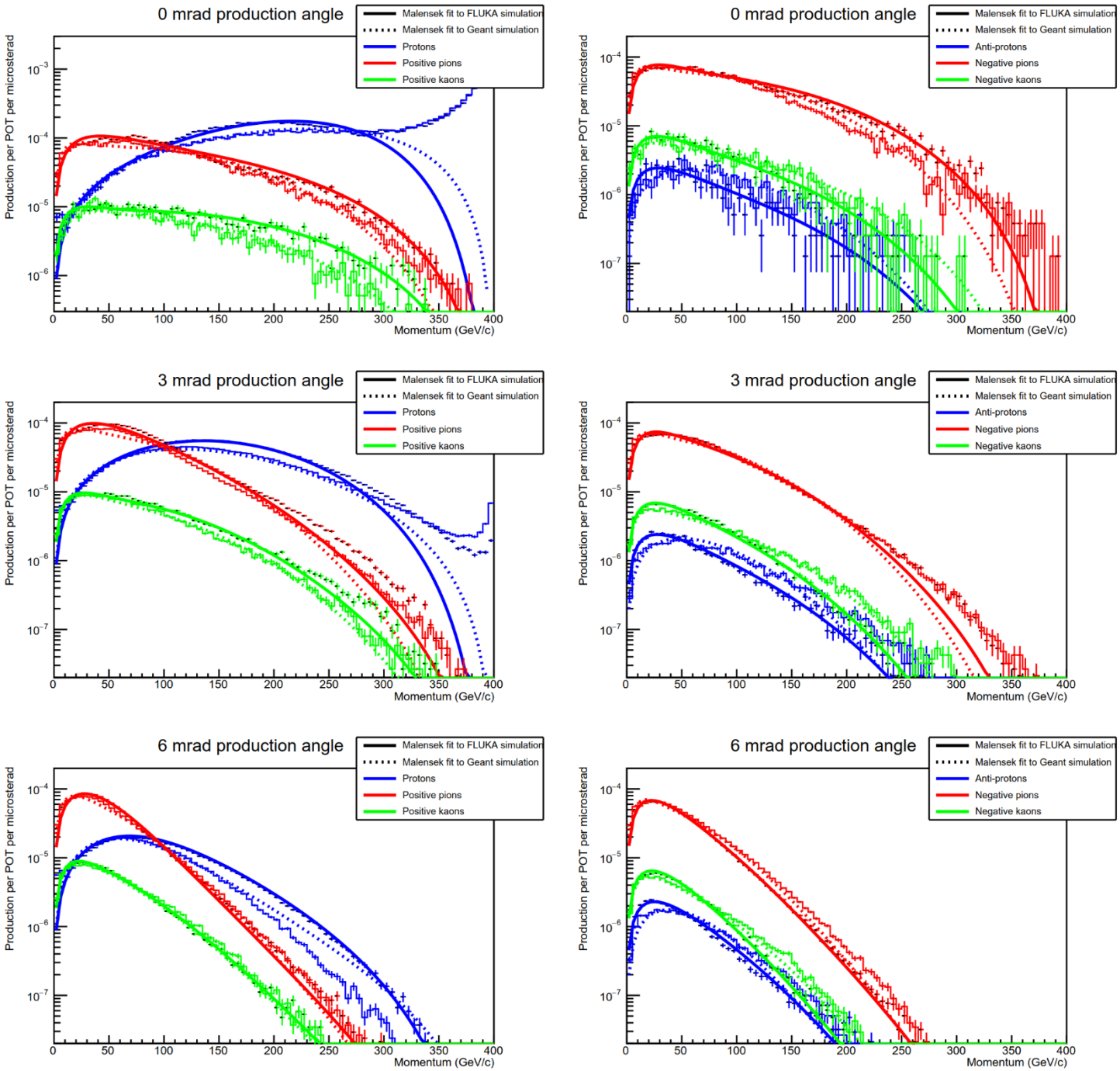

Figure 9: Sample of charged particles at several production angles, simulated in Geant (continuous histogram) and FLUKA (broken histogram), including Malensek fits to Geant data (dashed line) and to FLUKA data (solid line)

The fitted Malensek parametrizations give, in most cases, a reasonable approximation of the simulated distributions. There are several clear deviations. The primary component of the protons is deliberately excluded from the fit. The fits for the Geant data are for most plots somewhat worse than for FLUKA, particularly at higher momenta. This would indicate a difference in the underlying physics models, but without deep study no conclusion can be drawn on this. As a result, the conclusion should be that the parametrization can be a reasonable substitute depending on the application for doing the full simulation, but not an equivalent replacement.

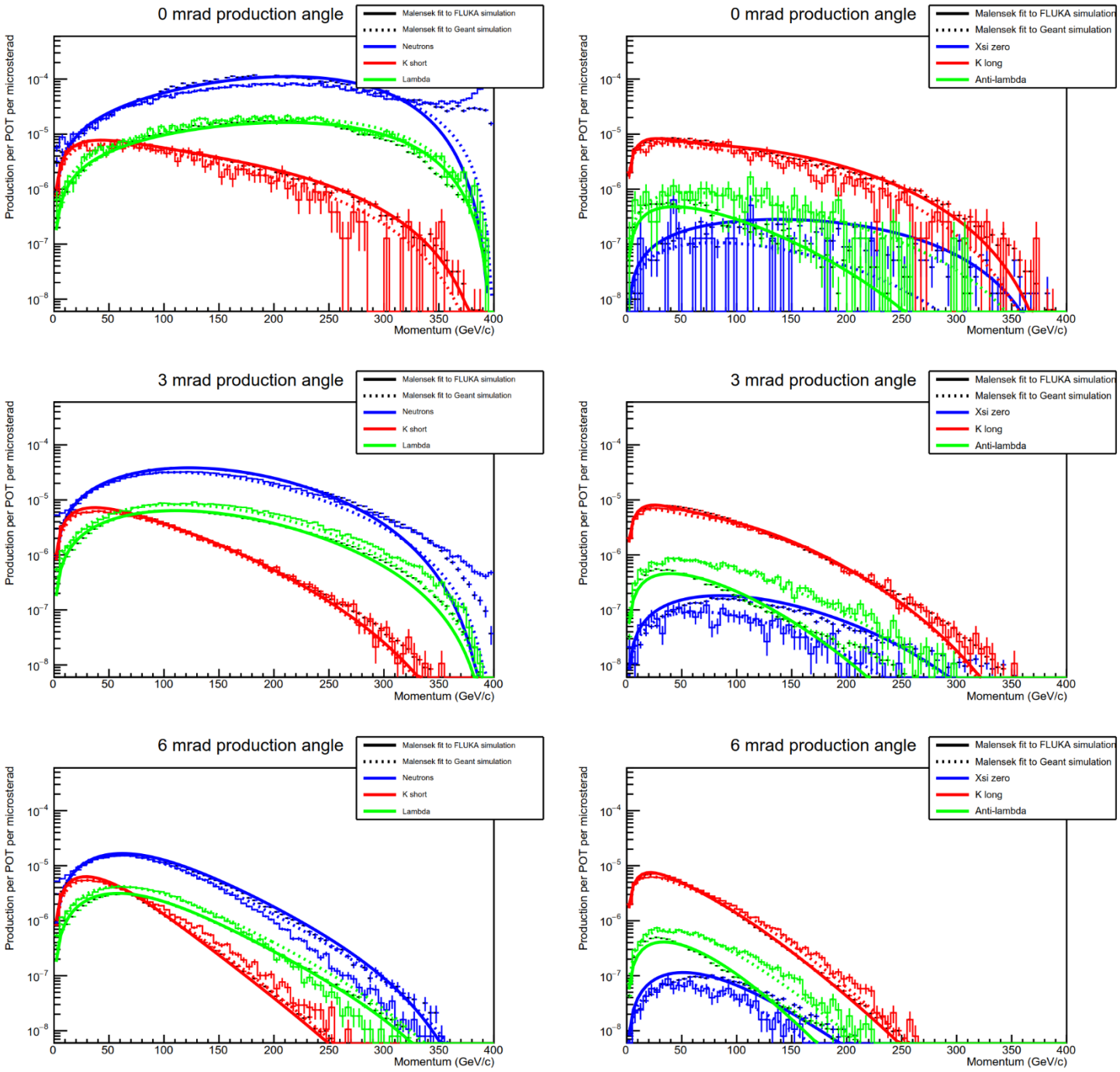

Figure 10: Sample of neutral particles at several production angles, simulated in Geant (continuous histogram) and FLUKA (broken histogram), including Malensek fits to Geant data (dashed line) and to FLUKA data (solid line)

From the simulations, it is clear that there is tension between Geant and FLUKA. Given the sparsity of available data, it is in many cases not clear whether FLUKA or Geant is closer to reality. The case of the $\overline{\Lambda^0}$ stands out – the disagreement between Geant and FLUKA is large, and data is available (see (7), (8)). Since the fraction of these events (relative to the Λ^0) is small, assessing its impact is left for later investigation.

Aside from the cases already pointed out, there is not usually more than a factor two between the results from FLUKA and Geant. This appears to be a reasonable measure for the intrinsic uncertainty of the curves that have been and will be presented. In further plots, usually the data from both simulations will be shown.

The final group of particles with a significant presence in the dataset are electrons, positrons and gammas (high-energy photons), forming over 60% of the total number of particles with a

momentum > 1 GeV/c. The generation mechanism dominating the production of these particles (electromagnetic) is very different from the hadronic processes discussed up until now. The Malensek parametrization intrinsically tails off to zero at low momentum, where the mechanisms for generation of electrons, positrons and photons lead to expecting an increasing population towards lower energies. As such, the Malensek parametrization is not computed for these particles. In further sections, the gamma flux will be described as a function of the production angle.

4 Target simulation results for KLEVER

This study was started for the purpose of investigating a range of possible choices for the KLEVER target, notably the material and the production angle. In the previous chapter, particle production was assessed for a beryllium target. It was found in earlier studies that changing the production angle from 2.4 mrad (initial choice for KLEVER production angle, following on from NA48) to 8 mrad would be highly beneficial in reducing the impact of background from Λ^0 baryons. Further backgrounds that will be studied as a function of production angle are neutrons and γ's.

4.1 Variation of particle incident angle

The production angle of particles sets the scale for both the signal and the background. As the production angle is shifted to higher values, the total production falls off for all particles, and their momentum spectrum softens. In Figure 11 and Figure 12, the mean and peak momentum are shown for K_L and Λ^0 as a function of the angle. In Figure 13, the absolute production rates are shown.

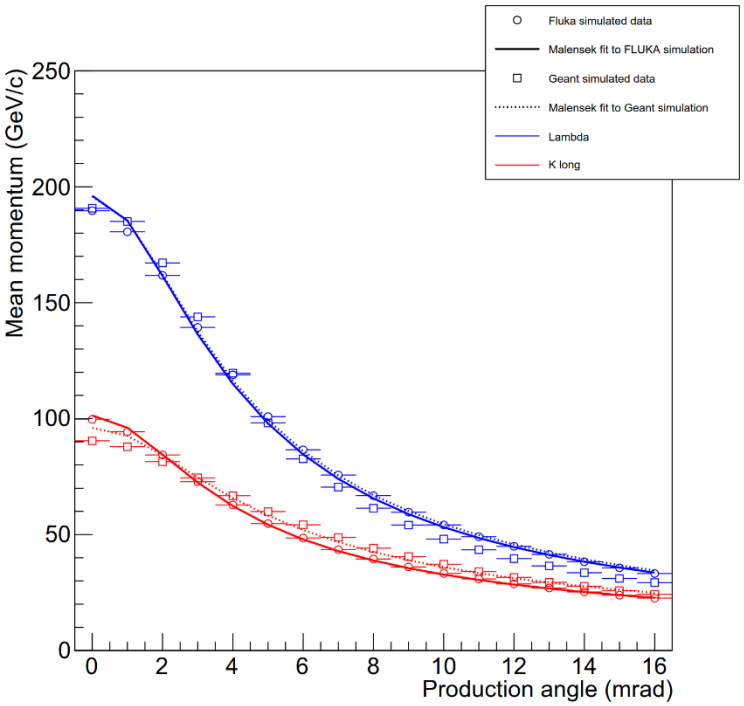

Figure 11: Mean momentum as found in FLUKA and Geant simulated data, and as derived from respective Malensek fits, as a function of production angle, for K_L and Λ^0

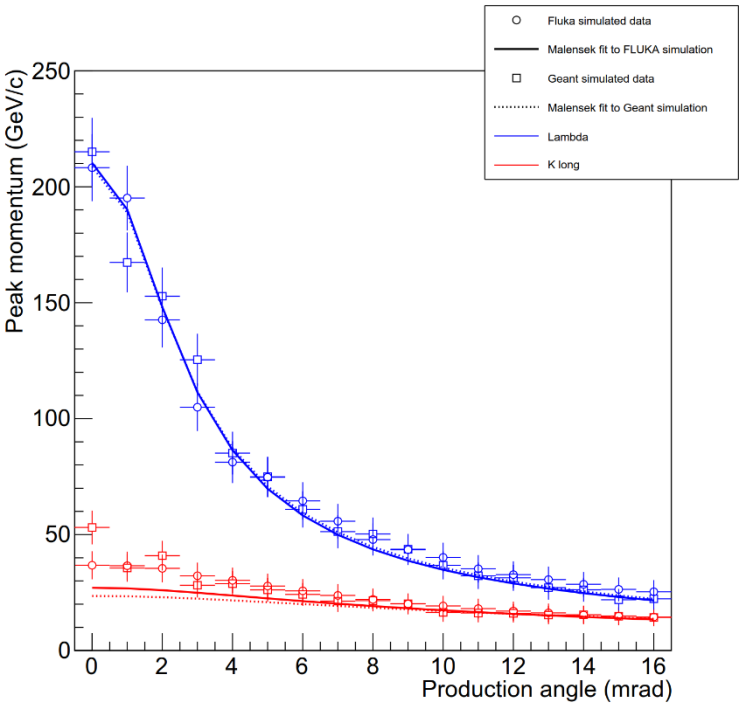

Figure 12: Peak momentum as found in FLUKA and Geant simulated data, and as derived from respective Malensek fits, as a function of production angle, for K_L and Λ^0

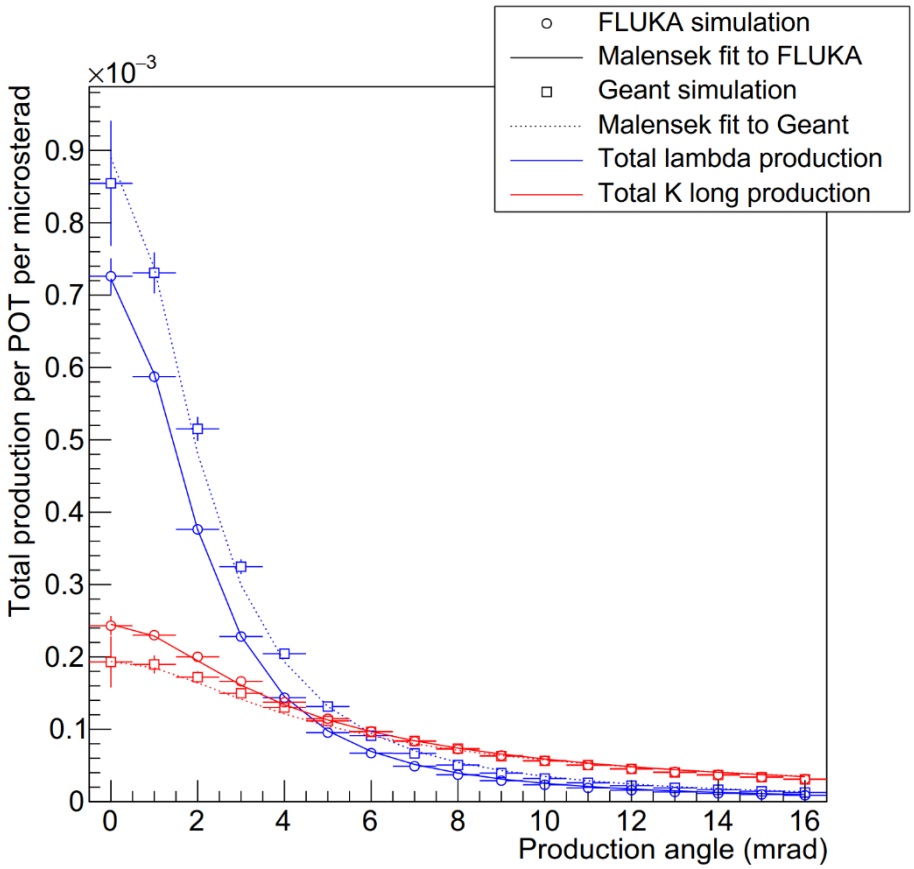

Figure 13: Total production of K_L and Λ^0 as a function of production angle, taken from FLUKA and Geant simulated data, and as integrated from the respective Malensek fits.

There is disagreement between FLUKA and Geant in terms of the absolute rate. As seen in Figure 13, FLUKA predicts more K_L and fewer Λ^0 than Geant does. In both codes the fall-off in rate is stronger for the Λ^0 than it is for the K_L, improving the signal to background ratio by about a factor 3. In Figure 14, the ratio of production of several background particles relative to the K_L as a function of the production angle is shown.

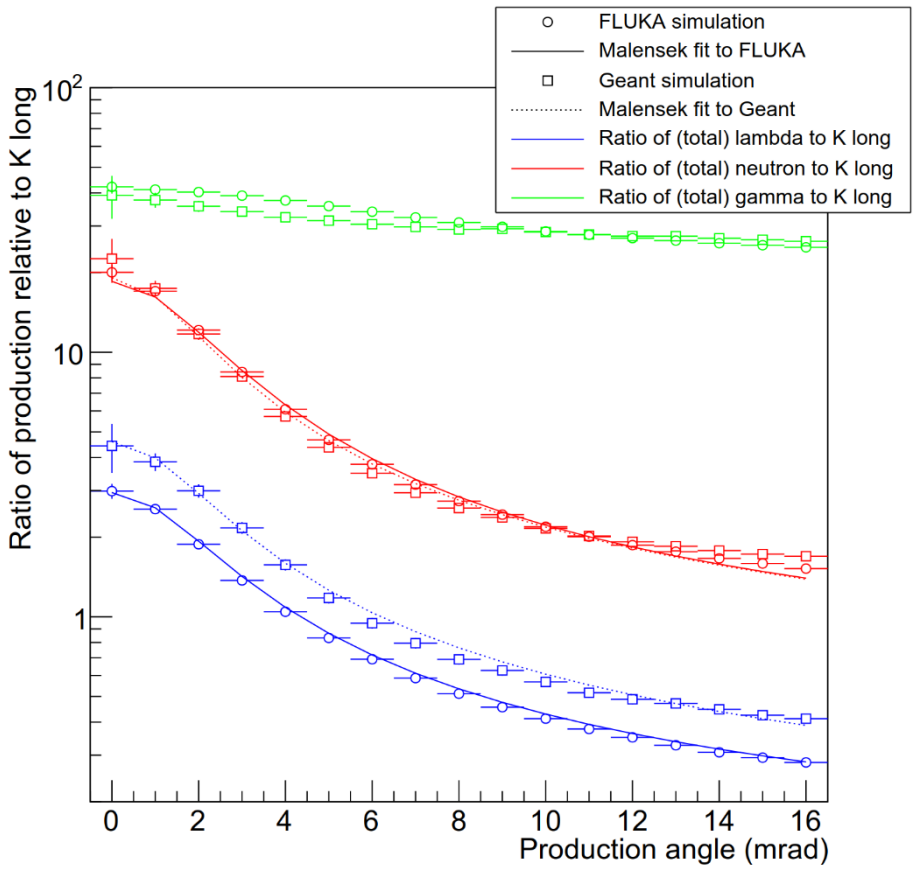

Figure 14: Ratio of production of Λ^0, neutrons and gamma to K_L. The momentum (energy) cut-off is set, for all particles, at 1 GeV/c.

The momentum softening observed with increasing angle (see Figure 11 and Figure 12) has a very different effect on Λ^0 and K_L. The lifetime of the Λ^0 is short (260 ps in the frame of rest), but still an appreciable fraction decays in the fiducial volume. The change from 2.4 to 8 mrad decreases the number of Λ^0 decays in the fiducial volume by about three orders of magnitude, mostly caused by the momentum softening. At the same time, the K_L momentum softens as well, but because of its long lifetime (about 51 ns in the frame of rest) the fraction decaying in the fiducial volume is still high, reducing only by about a third. The breakdown of the change in production and of the fraction decaying in the fiducial volume is shown in Table 2.

	Production		Decay fraction in FV	
	FLUKA	Geant	FLUKA	Geant
K_L (2.4 mrad)	1.87E-4	1.63E-4	3.66E-2	3.71E-2
K_L (8 mrad)	7.26E-5	7.33E-5	5.68E-2	5.61E-2
Λ^0 (2.4 mrad)	3.10E-4	4.31E-4	1.72E-4	1.79E-4
Λ^0 (8 mrad)	3.72E-5	5.06E-5	3.56E-6	4.25E-6

Table 2: Absolute production of K_L and Λ^0 (per POT, per microsteradian) and decay fraction in the fiducial volume.

To further show the impact, the Malensek parametrization for K_L and Λ^0 from FLUKA has been used, with the effect of decays added. The only assumption made for the beamline is that the fiducial volume was placed at 135 to 195 m from the target. The branching ratio for $\Lambda^0 \rightarrow n\pi^0$ is taken to be 0.358 (see (14)), and the Standard Model branching ratio of $K_L \rightarrow \pi^0 \nu\bar{\nu}$ is taken to be 3 10^{-11} (see (15)).

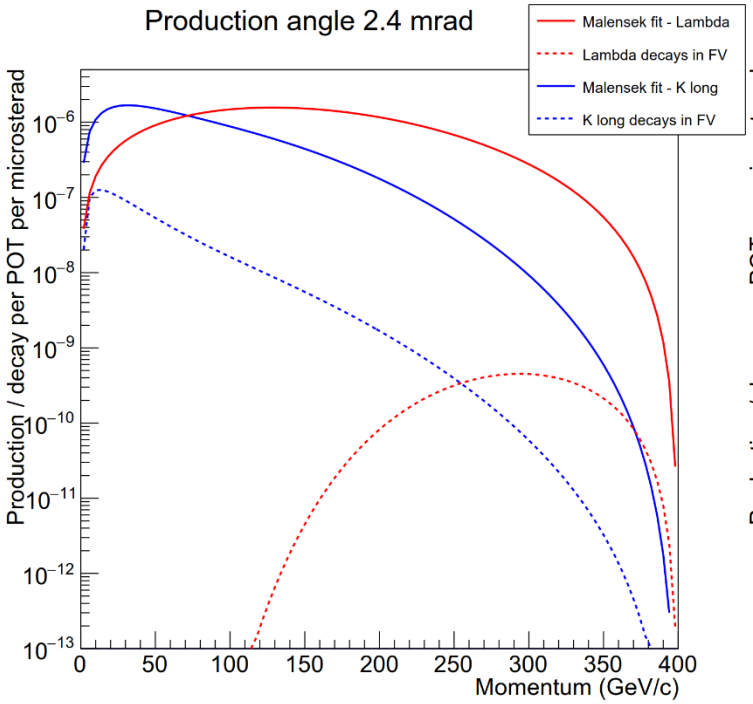

Figure 15: Production spectrum and spectrum of decays in fiducial volume, for K_L and Λ^0 at 2.4 mrad

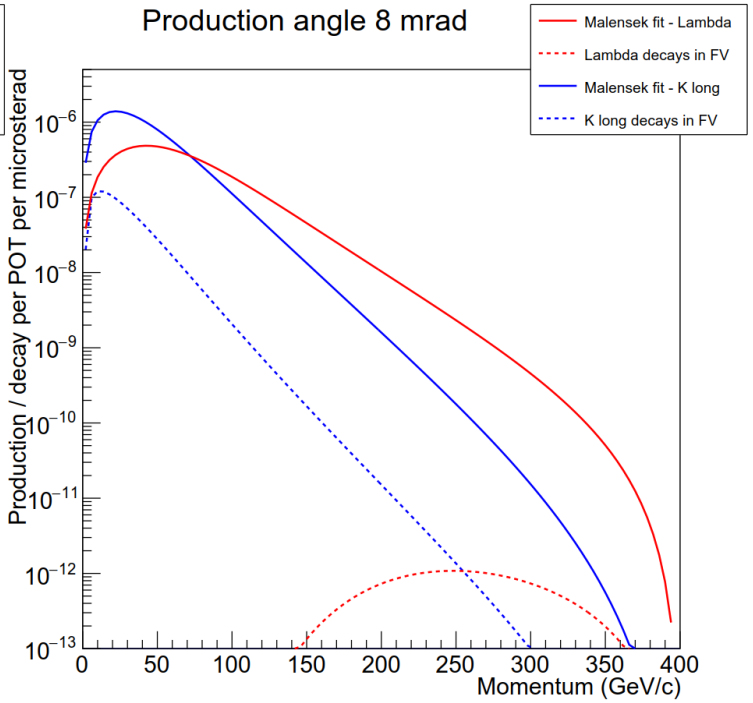

Figure 16: Production spectrum and spectrum of decays in fiducial volume, for K_L and Λ^0 at 8 mrad

It is clear that there is a strong reduction in the fraction decaying in the fiducial volume by moving from 2.4 to 8 mrad. At a production angle of 8 mrad, for an integrated intensity of 5 10^{19} protons on target, there will be about 1.3 10^9 decays of $\Lambda^0 \rightarrow n\pi^0$ in the fiducial volume. It has been shown that a series of kinematical cuts in the detector can give at least six orders of magnitude rejection of Λ^0 background, with the expectation that further tuning can reduce it to below signal level (about 50-100 detected signal decays are expected).

The number of neutrons and gammas produced by the target set the absolute rate at which the detector needs to operate. Table 3 lists some numbers for the absolute production at 2.4 and 8 mrad for neutrons and gammas for several energy limits.

	2.4 mrad Gamma		8 mrad Gamma		2.4 mrad Neutron		8 mrad Neutron	
	Fluka	Geant	Fluka	Geant	Fluka	Geant	Fluka	Geant
>1 GeV	7.43E-03	5.70E-03	2.24E-03	2.13E-03	1.94E-03	1.64E-03	1.99E-04	1.89E-04
>5 GeV	4.99E-03	3.82E-03	1.43E-03	1.36E-03	1.94E-03	1.64E-03	1.95E-04	1.84E-04
>15 GeV	3.36E-03	2.55E-03	7.51E-04	7.22E-04	1.93E-03	1.62E-03	1.86E-04	1.71E-04
>30 GeV	2.20E-03	1.63E-03	3.04E-04	3.17E-04	1.90E-03	1.59E-03	1.63E-04	1.45E-04

Table 3: Production of gammas and neutrons per proton on target per microsteradian, for several energy limits and production angles

4.2 Variation of target material

The simplest choice for the target material for KLEVER is to use beryllium (A=9.01), which is used for the current T10 target providing beam for NA62, and all of the CERN North Area target heads. Two other materials have been taken under consideration here, namely copper (A=63.5) and lead (A=207.2). In their pure forms, neither of these would be very suitable for making a target for KLEVER that could be adequately cooled and would stand up to the thermal conditions. In the case of copper, it is more likely that an alloy of copper, chrome and zirconium would be used (CuCrZr), which is already used for the dump material in the PS Booster (16), and was proposed to be used for the PS internal dump (17). This alloy is still 99% by weight copper, so the improved material properties easily outweigh the expected change in particle production. In the case of lead, it is likely that instead tungsten (A=183.8) would be used instead, for its superior mechanical and thermal properties.

The choice for these two materials in this target study was made because a reasonably comprehensive series of particle production studies is available, similar to what has been found for beryllium. The sources (7), (8) and (9) also contain comparable datasets for copper and lead. Benchmarks have also been performed for the particle species for which data is available, and have been included in Appendix B and Appendix C. To make a comparable target, the length was scaled relative to the nuclear interaction length of the material (see (14)), 421 mm for beryllium, 153.2 mm for copper and 175.9 mm for lead. For targets comparable to 400 mm beryllium, the full-length simulations were performed with 145.6 mm copper and 167.1 mm lead targets. The benchmarking tests were performed with 10% of that to prevent tertiary production from dominating. The parameters of the Malensek fits performed to the full-length copper and lead targets have also been included in the appendices.

Significant differences occur in particular at small production angles (i.e. less than 3 mrad), but at 8 mrad few of these are left, and there are only small differences (<20%) for hadron production between the various materials. Figure 17 and Figure 18 show the momentum spectra for Λ^0 and K_L.

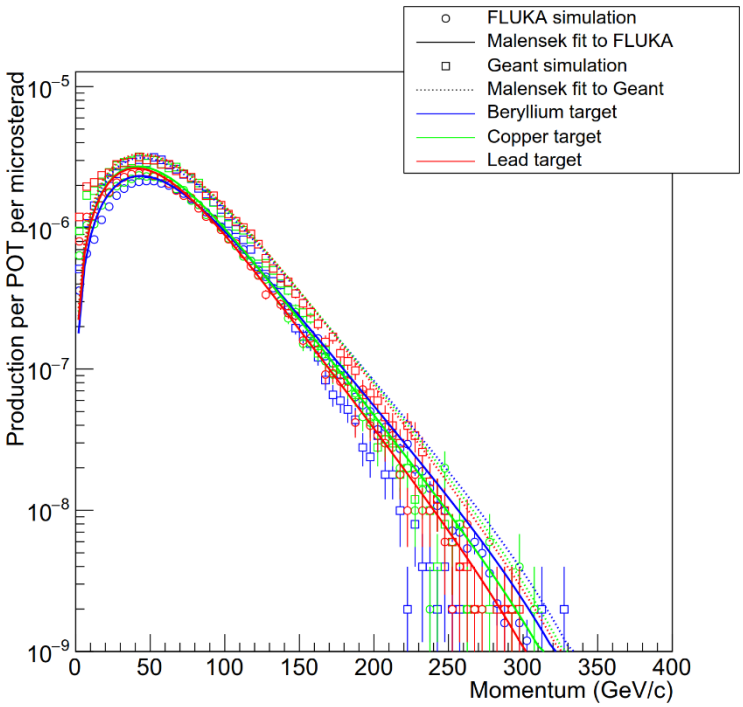

Figure 17: Λ^0 production spectrum per proton on target per microsteradian at 8 mrad production angle, for beryllium, copper and lead, including respective Malensek fits.

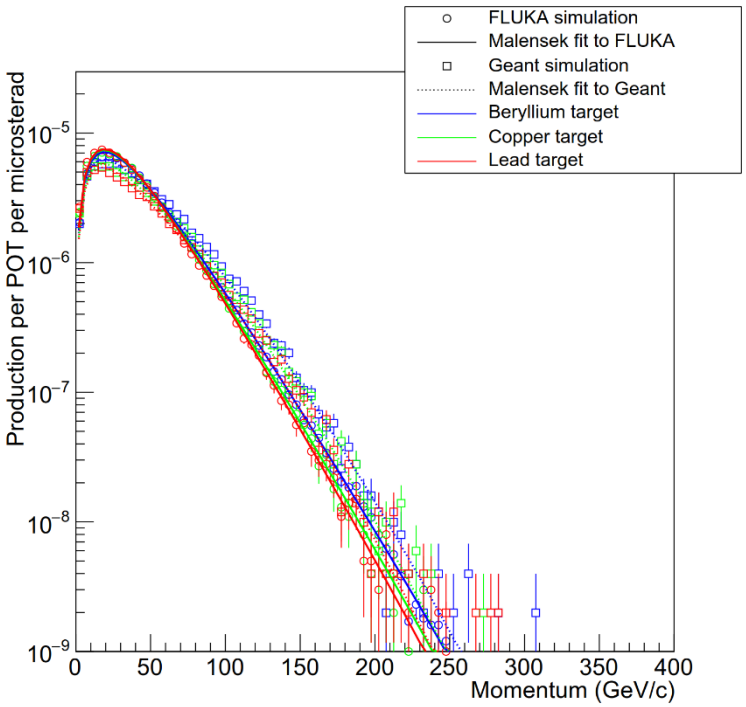

Figure 18: K_L production spectrum per proton on target per microsteradian at 8 mrad production angle, for beryllium, copper and lead, including respective Malensek fits.

The only large difference at 8 mrad between the materials was found to be the electromagnetic processes, where higher energy photons and e^+/e^- are highly suppressed. In Table 4, a brief overview is given of the number of photons and neutrons observed in simulation at 8 mrad production angle for several energy thresholds. The numbers listed are taken from FLUKA, but the numbers from Geant agree to within 10%. In Figure 19 and Figure 20, the full neutron and gamma spectra are shown.

	Gammas			Neutrons		
	Beryllium	Copper	Lead	Beryllium	Copper	Lead
>1 GeV	2.24E-03	2.36E-03	6.74E-04	1.99E-04	2.02E-04	2.07E-04
>5 GeV	1.43E-03	4.66E-04	1.38E-04	1.95E-04	1.99E-04	2.04E-04
>15 GeV	7.51E-04	1.44E-04	4.33E-05	1.86E-04	1.90E-04	1.94E-04
>30 GeV	3.04E-04	4.91E-05	1.47E-05	1.63E-04	1.64E-04	1.68E-04

Table 4: Production of gammas and neutrons per proton on target per microsteradian, for several materials, at a production angle of 8 mrad, taken from the FLUKA simulation.

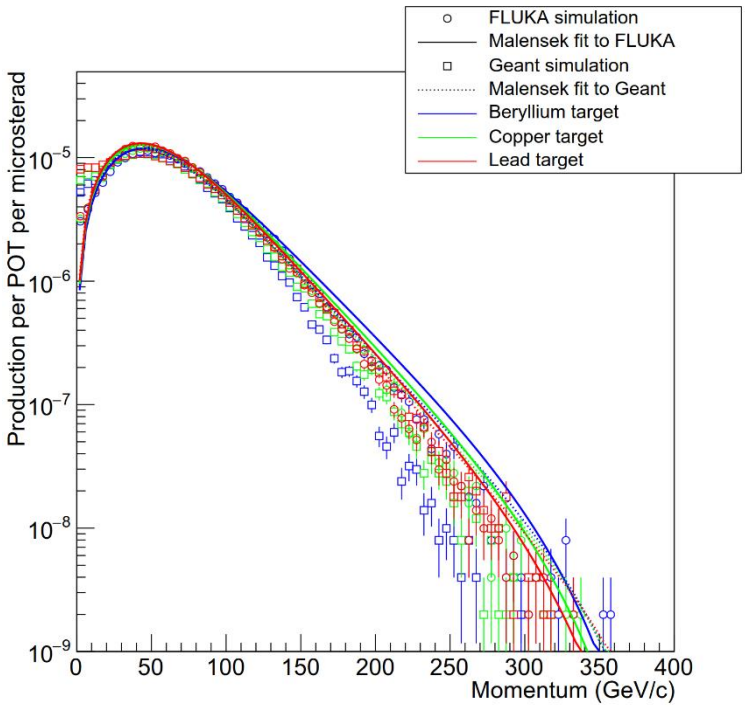

Figure 19: Neutron production spectrum per proton on target per microsteradian at 8 mrad production angle, for beryllium, copper and lead, including respective Malensek fits.

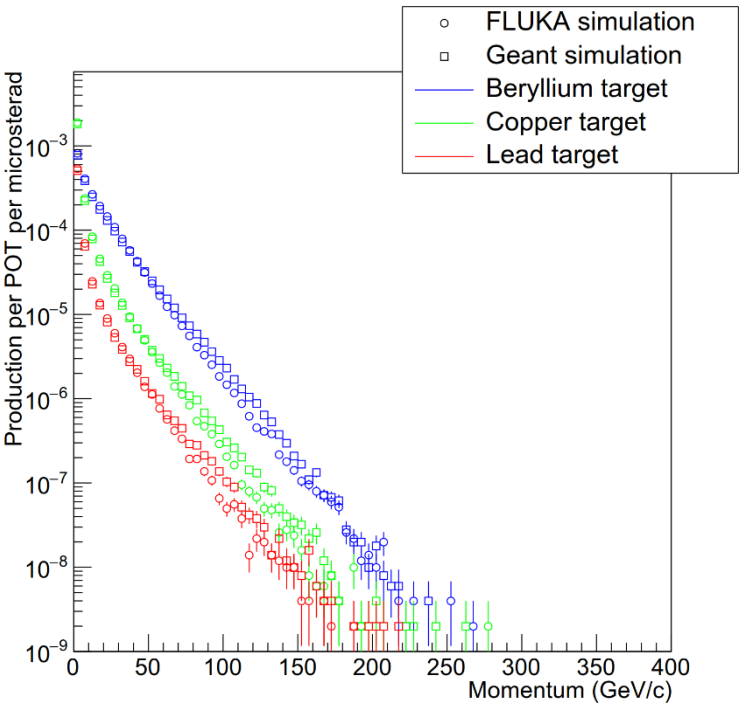

Figure 20: Gamma production spectrum per proton on target per microsteradian at 8 mrad production angle, for beryllium, copper and lead.

At an angle of 8 mrad, it appears that there is no significant difference in the neutron spectrum, fbut large differences are observed for the quantity of gammas. When including the relatively low energy gammas the total quantity appears similar, but the average energy is significantly lower for higher Z materials. Similar decreases are observed for the e^+/e^- spectra. This would indicate that further consideration of a high-Z target could be a tool for suppressing the quantity of gammas propagating to the detector. It is already foreseen that the flux necessitates a photon absorber in the beamline, which would also degrade the K_L passing through. A higher Z target would allow for a thinner photon absorber and would not degrade the beam as much. It is possible however that the potential for improvement from a high-Z target is completely outweighed by external factors, for example radiation protection, which would be much more problematic. These questions will be further revisited with a full beamline simulation.

Finally, it is interesting to also consider the variation of the production angle for the three different materials. In Figure 21 and Figure 22, the ratio to K_L is shown for Λ^0 and neutrons, and in Figure 23 the ratio of gamma to K_L is shown for several energy cuts. It appears that Geant shows some dependency on the material used – but the difference between materials observed in Geant is smaller than the difference between the same materials between Geant and FLUKA.

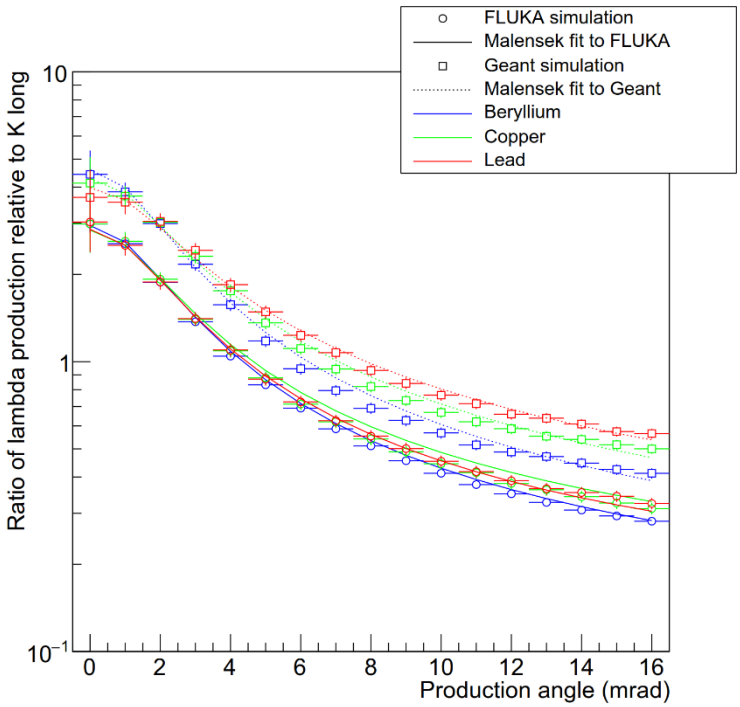

Figure 21: Ratio of Λ^0 production to K_L as a function of production angle, for several materials.

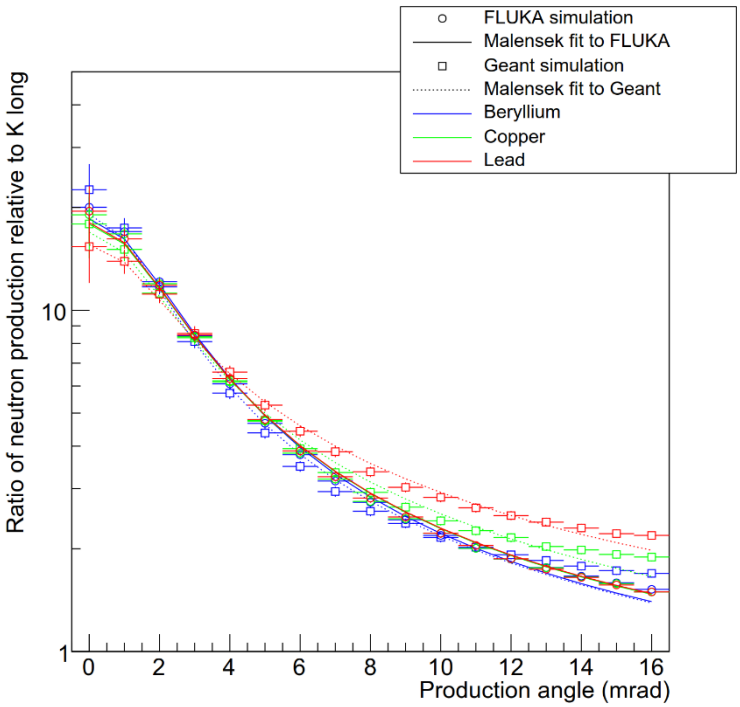

Figure 22: Ratio of neutron production to K_L as a function of production angle, for several materials.

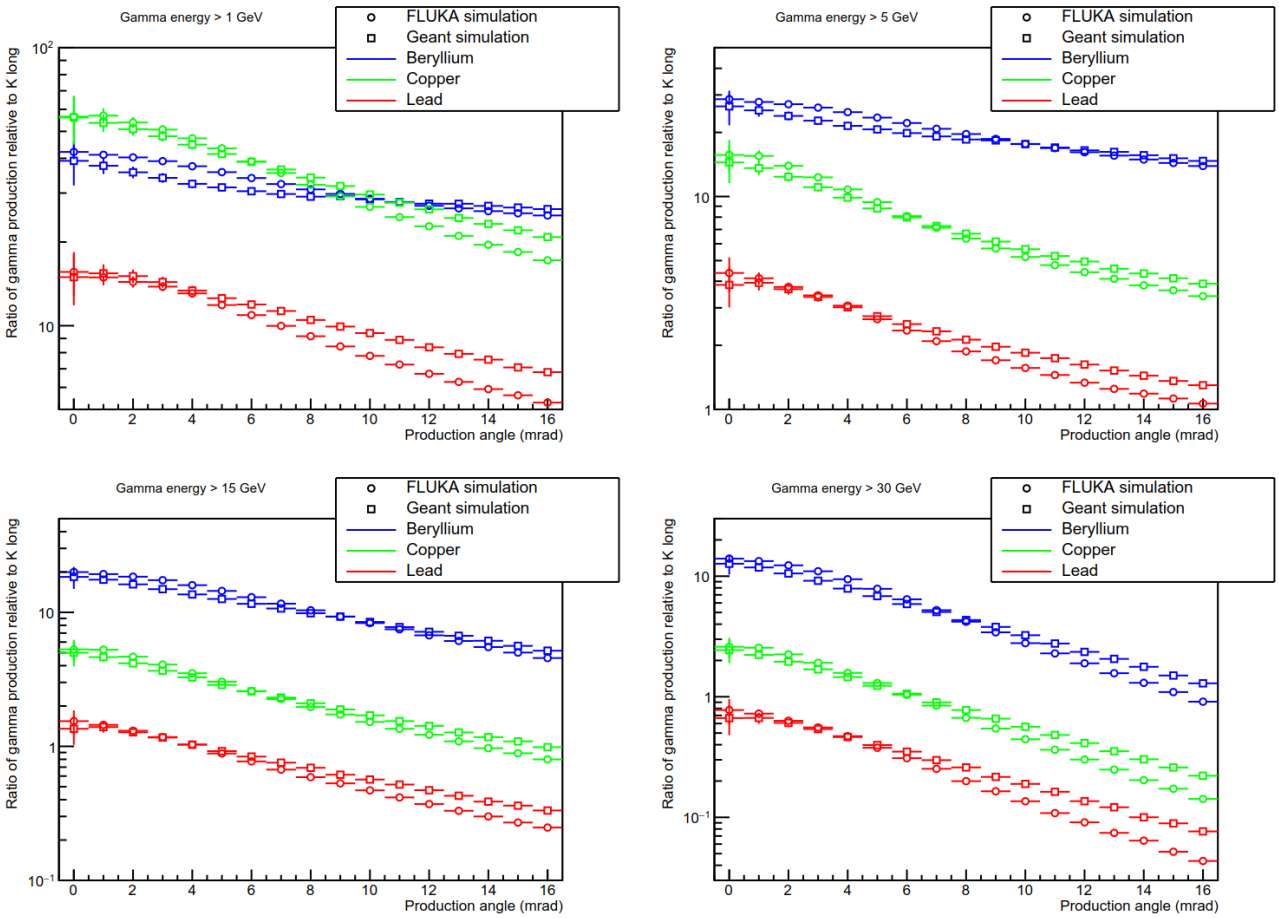

Figure 23: Ratio of gamma production to K_L as a function of production angle, for several energy cuts (only on the gamma) and for several materials.

4.3 Production at 8 mrad – full description

In the previous section, particle production was studied for targets over a range of production angles and materials. Figure 24 shows all the particles with a significant presence in the dataset, for a 400 mm beryllium target, at a production angle of 8 mrad. Particles that do not have a significant presence in the data because they are not produced directly in significant numbers (for example, muons) or because they decay almost immediately (for example, π^0) are not described.

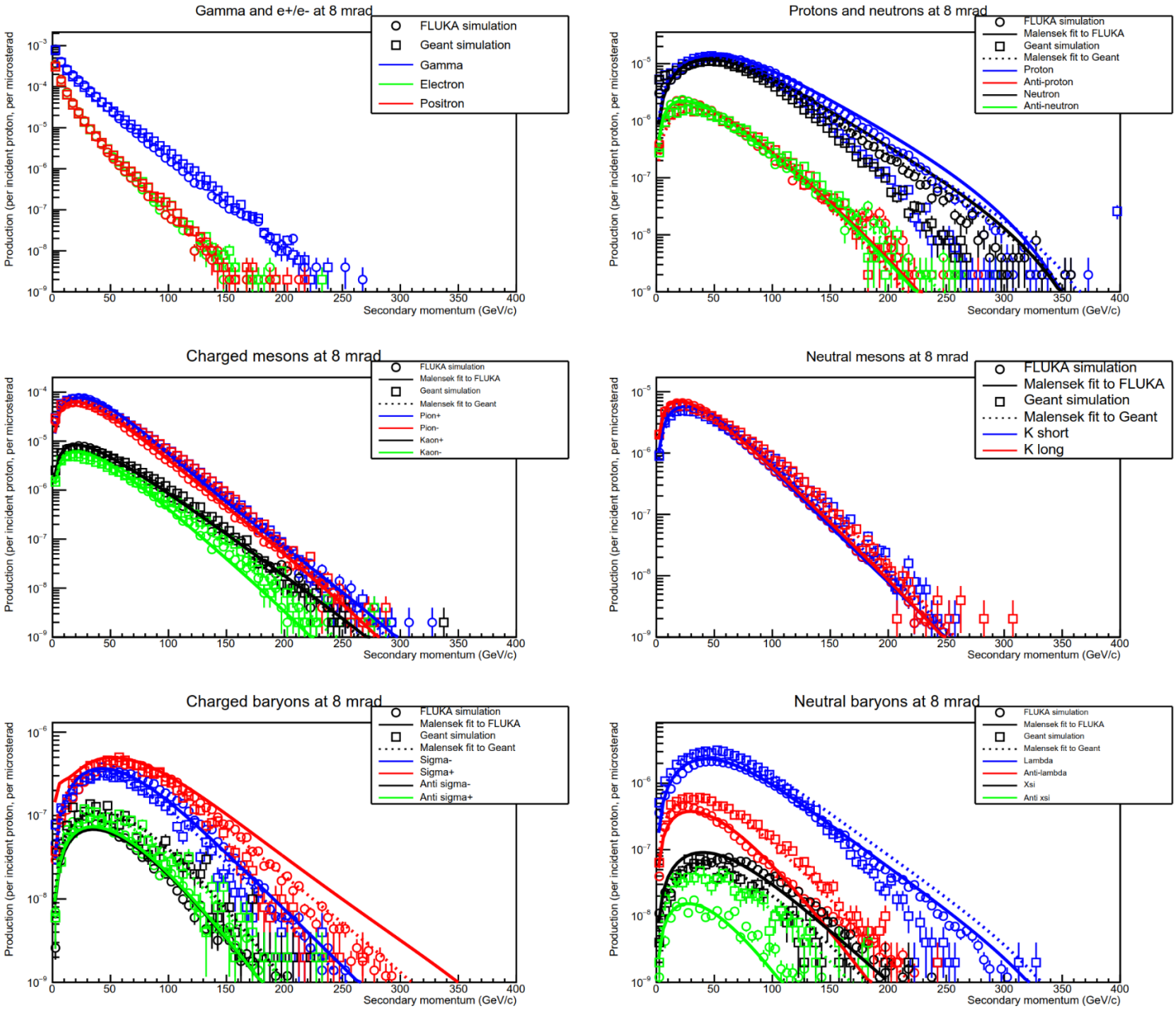

Figure 24: All particles with significant presence in the data sample, at 8 mrad production angle, for a 400 mm Beryllium target

5 Conclusions

An assessment has been made of particle production for the proposed KLEVER experiment. The production from a beryllium target was assessed in terms of the production angle, target length and target material.

The target was simulated in both Geant and FLUKA. Neither performs consistently better in the benchmark relative to the data that has been taken under consideration. At extreme angles (below 2 mrad and above 12 mrad), for Λ^0 and K_S experimental data is not well replicated in either, for intermediate angles both perform reasonably. The experimental data for neutron production disagrees with both simulations, with the simulations overproducing neutrons by a factor of about 2 to 5. The simulated data was presented for both Geant and FLUKA, ending in the conclusion that no large deviations between the two are found. It is worth noting that there is consistently more Λ^0 and less K_L in Geant, leading to a Λ^0 / K_L ratio that is consistently about 40% higher in Geant.

A new parametrization, the Malensek parametrization, was presented to allow for rapid, simple replication of the simulated data. It was found that this parametrization is in most cases a reasonable representation of the simulated data. Fits were made to the data using ROOT, and the fit parameters have been made available in Appendix A.

The initial design of the KLEVER experiment used the same production angle as NA48, which has been revised to 8 mrad. It has been shown that from the simulation it is expected that this increase has a small effect on the signal (reducing the number of K_L decays in the fiducial volume by about a third). Simultaneously it has a large effect on the background from Λ^0, for which the decays in the fiducial volume are reduced by about a factor 370. The shift to an 8 mrad production angle thus has the intended effect of significantly reducing the expected background from Λ^0. To bring this background fully under control, between seven and nine orders of magnitude rejection are then required. It has previously been demonstrated that six orders of magnitude rejection can be achieved relatively easily by means of kinematic cuts. The expectation is that the rest is within reach, by tuning the transverse momentum and decay angle cuts further. The background caused by neutrons and gammas has been quantified, and will serve as further input for the design of the KLEVER detector and beamline.

Finally, two other materials have been benchmarked (see Appendix B) and assessed in terms of particle production. No large deviations are observed in the simulation between the various materials, using targets of comparable nuclear interaction length, excepting the gamma and electron spectra. Relative to a beryllium target, depending on the energy cut, the copper target produces up to a factor six fewer photons. A lead target produces between three and twenty times fewer photons, leading to a much looser requirement on the photon absorber, improving the beam quality. Although the gamma reductions are significant, it is not clear that a higher Z target would necessarily be a better choice, in particular for radiation protection. It is foreseen that more information can be extracted from a full beamline simulation.

Acknowledgements

This document could not have been written without the continuous help of the colleagues of the EN-EA-LE section, in particular Lau Gatignon and Niels Doble. Additionally, many thanks to Matthew Moulson for investing valuable time and effort in guiding this study.

This research project has been supported by a Marie Skłodowska-Curie COFUND project of the European Commission's Horizon 2020 Programme under contract number 665779 COFUND

6 References

1. *Prospects for an experiment to measure BR(KL→π0νν) at the CERN SPS.* **Moulson, M.** 2016.

2. *The FLUKA Code: Developments and Challenges for High Energy and Medical Applications.* **Böhlen, T.T., et al.** s.l. : Nuclear Data Sheets 120, 211-214, 2014.

3. *FLUKA: a multi-particle transport code.* **Ferrari, A., et al.** s.l. : CERN-2005-10 (2005), INFN/TC_05/11, SLAC-R-773.

4. *G4beamline simulation program for matter-dominated beamlines.* **Roberts, T.J. and Kaplan, D.M.** s.l. : Proceedings of PAC07, Albuquerque, New Mexico, USA, 2008.

5. *Recent developments in Geant4.* **Allison, J. et al.** s.l. : Nucl. Inst. & Meth. in Phys. Res. A, 2016, Vol. 835, pp. 186-225.

6. *Precise measurements of particle production by 400 GeV/c protons on beryllium targets.* **Atherton, H.W., et al.** s.l. : CERN 80-07, 1980.

7. **Lundberg, B.G.** *Neutral strange particle production and polarization at large pT.* s.l. : University of Wisconsin-Madison, 1984. Fermilab-thesis-1984-16.

8. *Production of Ξ0 and Ξ0b hyperons by 400-GeV protons.* **Beretvas, A., et al.** 1, s.l. : Physical Review D, 1986, Vol. 34, pp. 53-74.

9. *Inclusive Neutron Production.* **Jones, L.W., et al.** s.l. : 16th International Cosmic Ray Conference, Vol. 6, 1979.

10. *ROOT - An Object Oriented Data Analysis Framework.* **Brun, R. and Rademakers, F.** s.l. : Proceedings AIHENP'96 Workshop, Nucl. Inst. & Meth. in Phys. Res. A, 1997. Vol. 389, pp. 81-86.

11. *Empirical formula for thick target particle production.* **Malensek, A.J.** s.l. : Fermilab-FN-341, 1981.

12. *Strangeness Production in High-Energy Proton-Nucleus Collision.* **Luk, K.B.** s.l. : Fermilab-CONF-89/040, 1988. Hadronic matter in collision, 3rd meeting.

13. *High-Energy collisions with atomic nuclei: The experimental results.* **Frederiksson, S., et al.** s.l. : PHYSICS REPORTS (Review Section of Physics Letters), 1987. Vol. 144, pp. 187-320.

14. **The Particle Data Group Collaboration.** *Review of Particle Physics.* s.l. : Chin. Phys., 2016. Vol. C40.

15. *K+→π+νν and KL→π0νν in the Standard Model: Status and Perspectives.* **Buras, A.J., et al.** s.l. : JHEP 1511, 2015, Vol. 033.

16. *Design of air-cooled beam dump for extraction line of PS Booster.* **Perillo-Marcone, A., et al.** s.l. : Proceedings of IPAC2013, Shanghai, China. THPFI062.

17. **Esala, J.** *Preliminary design of the new Proton Synchrotron Internal Dump core.* s.l. : CERN-THESIS-2017-330, 2017.

Appendix A: Malensek fit parameters extracted from Geant and FLUKA, for a 400mm beryllium target

	Fluka				Geant			
	A	B	C	D	A	B	C	D
Proton	4.53862	5.77814	0.821462	-8.01925	2.26667	6.99293	0.746749	-3.85445
Anti-proton	5.62613	3.24427	1.61419	11.4827	6.83823	1.34215	1.09007	-1.15579
Neutron	3.58473	5.56433	0.798356	-5.86517	2.44021	6.11583	0.792989	-3.43338
Anti-neutron	5.61998	3.30208	1.52615	11.5805	3.69546	2.49687	1.34839	13.9507
Pion+	2.9279	99.9893	0.686501	9.69059	3.94716	164.177	0.771582	23.3638
Pion-	3.85317	107.178	0.747812	15.2911	4.91012	155.491	0.936827	24.939
Kaon+	2.82915	14.4555	0.823401	17.943	3.4906	13.403	0.974752	17.1019
Kaon-	5.41013	9.96711	0.966803	13.124	4.57199	9.69416	1.08487	19.4121
K short	3.02378	7.03651	0.81706	9.03933	3.26307	5.58656	1.02974	7.7298
K long	3.70486	12.9225	0.816712	18.2055	4.166	12.4605	1.1024	21.442
Lambda	2.65557	1.18492	0.814228	-3.79619	2.44773	1.56483	0.876035	-3.31343
Anti-lambda	5.76952	0.390079	1.30269	3.58575	3.07613	0.557426	1.1492	4.76029
Sigma-	1.53724	0.208695	1.04433	0.0410302	1.9067	0.172769	1.00822	-0.550076
Sigma+	0.415236	1.34039	1.29292	83.0601	1.46969	0.214497	0.999157	-2.16208
Anti-sigma-	3.93291	0.0592135	1.75948	4.07683	4.20345	0.0773912	1.51657	0.326826
Anti-sigma+	4.12229	0.0651141	1.80333	4.22731	4.08893	0.0629718	1.50512	0.202292
Xsi zero	3.26362	0.0544842	0.886351	-2.2658	4.30754	0.0425393	1.26654	-0.508494
Anti xsi zero	6.25764	0.0163828	0.88562	2.26325	4.66667	0.0281292	1.3063	-0.392093
Xsi-	7.28287	0.03077	1.20968	-7.5342	8.3856	0.0349433	1.21708	-6.17819
Anti-xsi+	7.70745	0.00662314	1.16222	-2.67645	8.92393	0.0131987	1.59373	-8.07794

Table 5: Malensek parameters for a beryllium target (see Section 3.2 for further details) for particles with a significant presence in the simulated Geant and FLUKA datasets.

`Appendix B: Benchmarking of a copper target

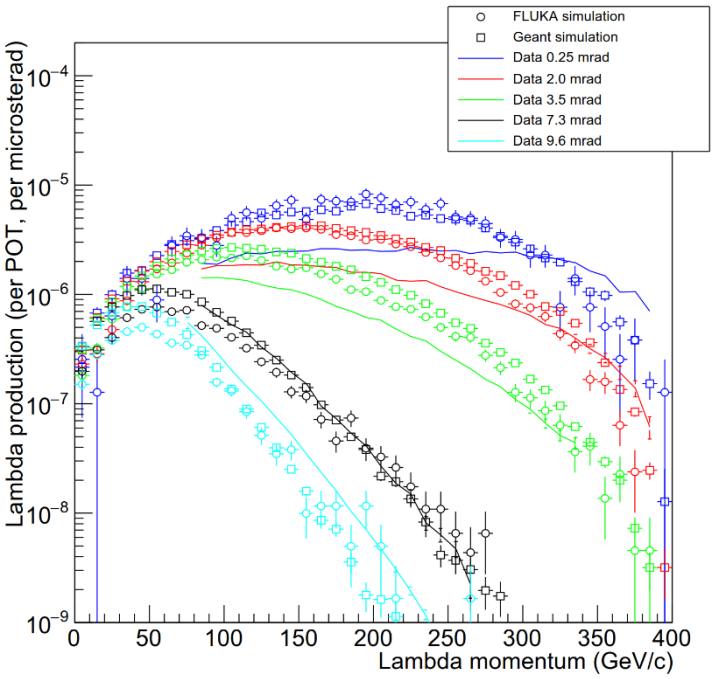

Figure 25: Production of Λ^0 as measured (solid lines, data from (8)) and as simulated in FLUKA and Geant for a copper target

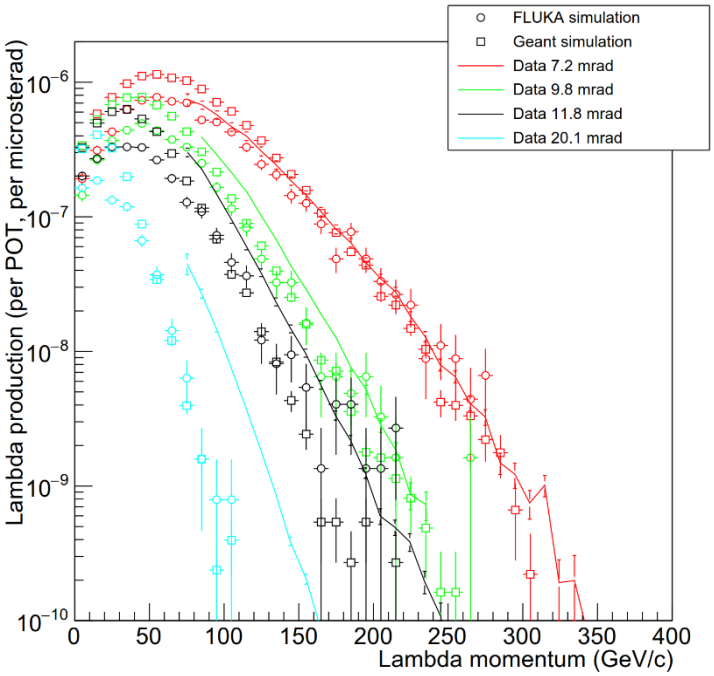

Figure 26: Production of Λ^0 as measured (solid lines, data from (7)) and as simulated in FLUKA and Geant for a copper target

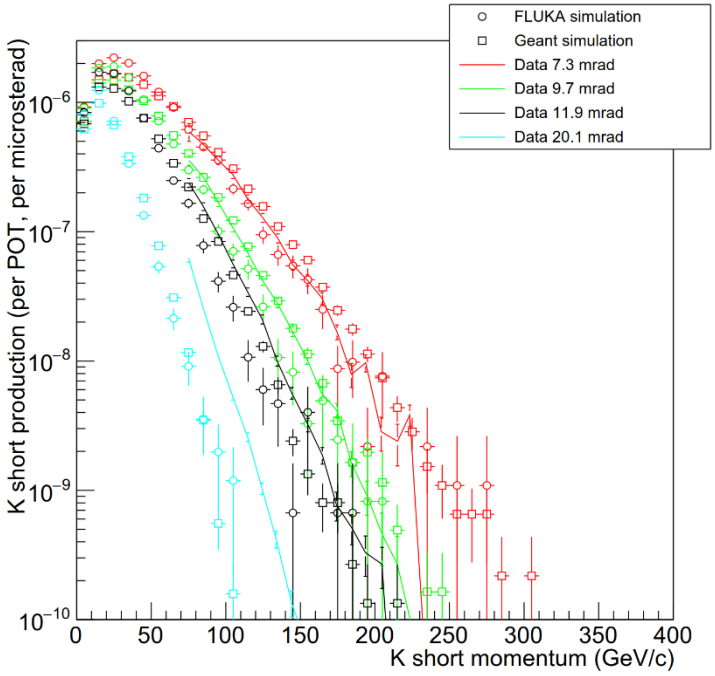

Figure 27: Production of K_s as measured (solid lines, data from (7)) and as simulated in FLUKA and Geant for a copper target

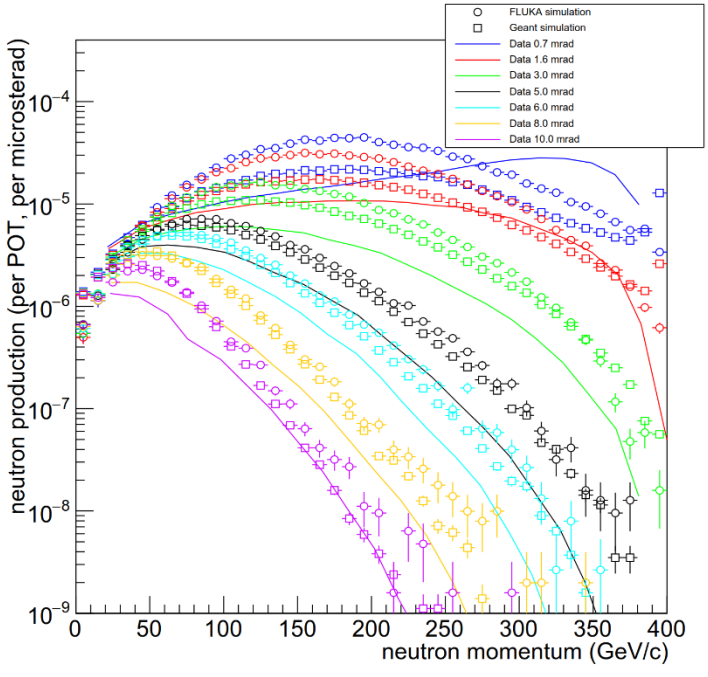

Figure 28: Production of neutrons as measured (solid lines, data from (9)) and as simulated in FLUKA and Geant for a copper target

	Fluka				Geant			
	A	B	C	D	A	B	C	D
Proton	4.82802	6.4996	0.816848	-7.98552	1.49198	7.85105	0.853215	-1.59662
Anti-proton	5.8728	3.38916	1.51033	12.6166	6.55294	1.48533	1.17227	0.373226
Neutron	3.65846	6.31483	0.773233	-5.52281	1.91172	6.67155	0.881277	-1.6458
Anti-neutron	5.78773	3.38257	1.43469	12.0831	4.73224	3.80058	1.39986	23.2629
Pion+	3.35454	115.04	0.687882	12.0366	4.73114	162.82	0.851523	24.2309
Pion-	4.47337	127.422	0.741936	19.0755	5.62944	166.044	0.996608	27.8496
Kaon+	3.02706	14.4586	0.799468	17.161	3.98599	12.2348	1.0741	17.0163
Kaon-	5.98121	10.3347	0.962731	12.8212	5.21228	8.99607	1.1601	21.1327
K short	3.63393	9.97905	0.785487	12.6833	4.06706	8.28465	1.13548	15.3992
K long	4.046	13.4457	0.782724	17.645	4.69827	11.6997	1.13972	21.1225
Lambda	2.67051	1.48585	0.802699	-3.12946	2.40159	1.70003	0.962115	-2.43252
Anti-lambda	6.19251	0.785864	1.44835	10.9171	5.17319	0.552619	1.22858	1.58594
Sigma-	1.98502	0.252269	1.06554	0.142231	4.01734	0.140296	1.05779	-3.75364
Sigma+	1.87746	0.153946	-1348.94	-0.481408	1.03361	1.7343	1.19098	72.2548
Anti-sigma-	5.36367	0.0999667	1.67049	4.95558	4.27817	0.0879919	1.65246	1.30147
Anti-sigma+	4.08125	0.0846262	1.39126	4.53714	4.12407	0.0773622	1.41252	0.974471
Xsi zero	3.46544	0.0432297	1.22367	-1.89352	4.3273	0.0357885	1.50357	-0.354898
Anti xsi zero	6.61179	0.019358	1.30562	6.44647	4.18218	0.0184096	1.47085	-0.708276
Xsi-	7.35385	0.0340226	1.12475	-7.33078	8.47884	0.0299135	1.44003	-6.01131
Anti-xsi+	8.04235	0.00789625	1.3186	-2.24168	9.48254	0.0219095	1.57661	-6.46615

Table 6: Malensek parameters for a copper target (see Section 3.2 for further details) for particles with a significant presence in the simulated Geant and FLUKA datasets.

Appendix C: Benchmarking of a lead target

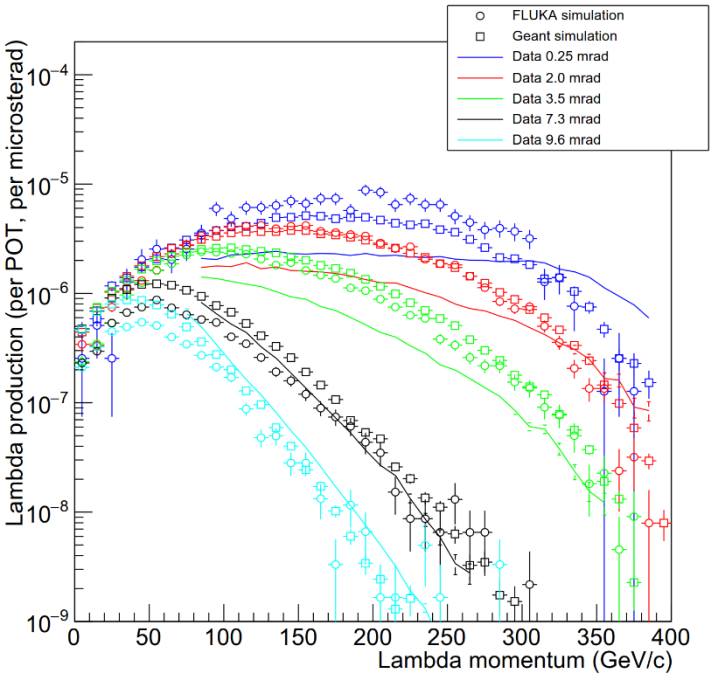

Figure 29: Production of Λ^0 as measured (solid lines, data from (8)) and as simulated in FLUKA and Geant for a lead target

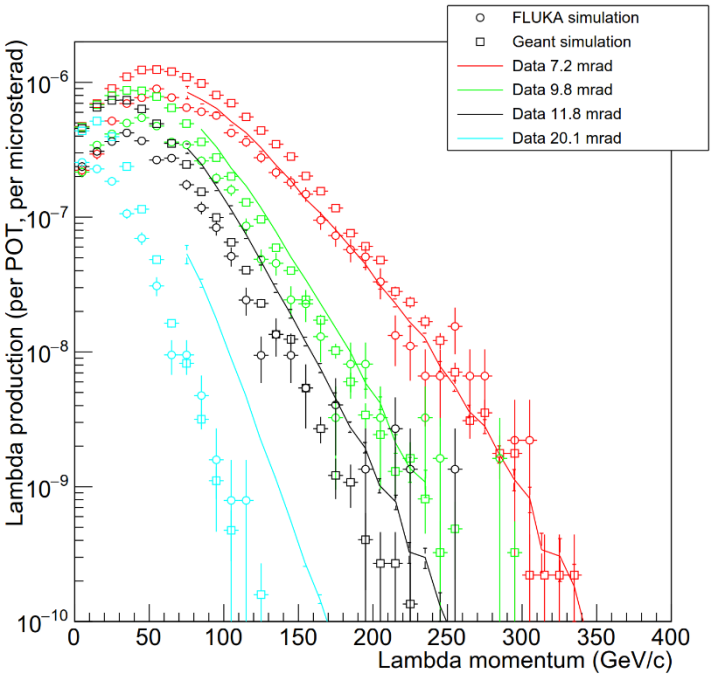

Figure 30: Production of Λ^0 as measured (solid lines, data from (7)) and as simulated in FLUKA and Geant for a lead target

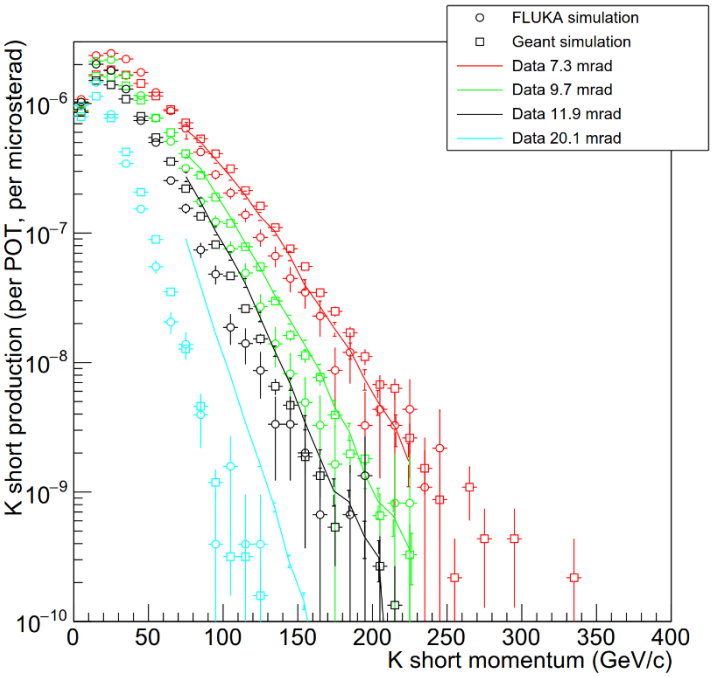

Figure 31: Production of K_s as measured (solid lines, data from (7)) and as simulated in FLUKA and Geant for a lead target

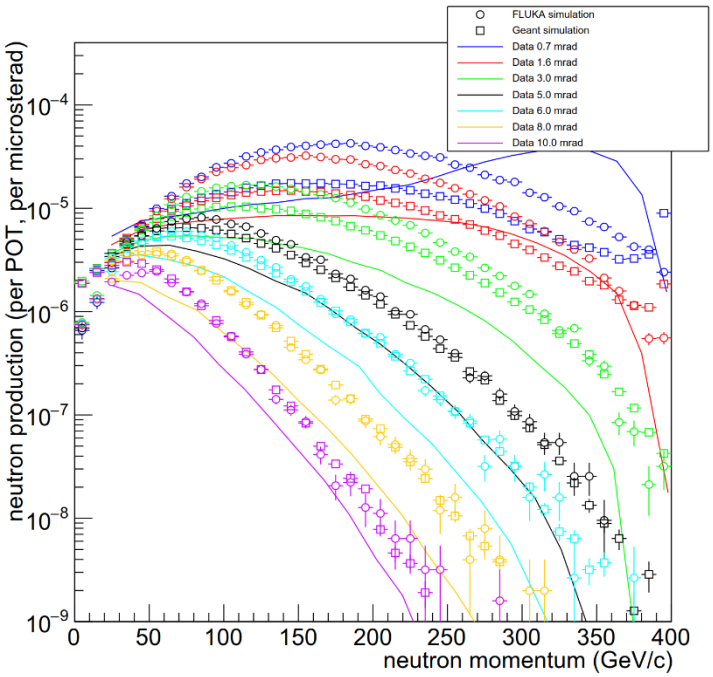

Figure 32: Production of neutrons as measured (solid lines, data from (9)) and as simulated in FLUKA and Geant for a lead target

	Fluka				Geant			
	A	B	C	D	A	B	C	D
Proton	5.07218	6.88007	0.827416	-7.99724	0.989132	8.43023	0.952995	0.208982
Anti-proton	6.27174	3.15957	1.5363	11.3109	7.11114	1.74015	1.21909	0.963309
Neutron	3.84041	6.68693	0.761117	-5.51946	1.3665	7.51432	0.958243	0.244751
Anti-neutron	6.19422	3.3241	1.3697	11.1849	5.14222	4.02079	1.41987	22.2768
Pion+	3.79358	129.298	0.71072	14.5517	5.44958	168.622	0.911629	26.5271
Pion-	4.99549	143.678	0.744818	22.3266	6.13324	172.212	1.04049	29.3777
Kaon+	3.2045	14.3069	0.783246	16.93	5.01108	15.1434	1.1471	25.3577
Kaon-	6.29234	10.6239	0.934476	13.1027	5.97497	8.01698	1.33019	20.5498
K short	3.92046	10.0147	0.783422	12.4491	4.64227	7.84492	1.22732	15.7436
K long	4.42055	13.5627	0.79757	16.9479	5.19961	11.3312	1.1601	21.4385
Lambda	3.15087	1.47973	0.760871	-3.71317	2.18093	1.8033	1.04519	-1.35378
Anti-lambda	6.71031	0.61499	1.28733	5.44005	4.19735	0.71908	1.21537	5.76595
Sigma-	4.00184	0.169412	1.06383	-3.92185	5.10472	0.170454	1.20359	-4.57225
Sigma+	2.20489	0.230657	1.22315	-2.7211	1.17331	1.55149	1.32689	115.193
Anti-sigma-	5.06045	0.0950986	1.79262	5.89474	4.09722	0.0862921	1.79359	2.36965
Anti-sigma+	5.37338	0.0988689	1.55534	4.76813	4.16201	0.0900052	1.46444	2.18455
Xsi zero	3.46805	0.0444666	1.26078	-1.57572	4.84554	0.038625	1.38325	0.129073
Anti xsi zero	6.01215	0.0255539	0.38402	2.35302	4.7175	0.0248496	1.42224	0.393485
Xsi-	7.36857	0.0329821	1.10997	-7.2872	8.68001	0.0276232	1.54103	-5.77756
Anti-xsi+	10.2403	0.015563	1.97084	-1.17791	9.27373	0.0172661	1.69399	-6.61444

Table 7: Malensek parameters for a lead target (see Section 3.2 for further details) for particles with a significant presence in the simulated Geant and FLUKA datasets.